Visualizing Second Order Tensor Fields with Hyperstreamlines

Thierry Delmarcelle and Lambertus Hesselink

Stanford University

March 15, 1993

Abstract

Hyperstreamlines are a generalization to second order tensor fields of the conventional streamlines used in vector field visualization. As opposed to point icons commonly used in visualizing tensor fields, hyperstreamlines form a continuous representation of the complete tensor information along a three-dimensional path. This technique is useful in visualizing both symmetric and unsymmetric three-dimensional tensor data. Several examples of tensor field visualization in solid materials and fluid flows are provided.

keywords - *scientific visualization, multivariate data visualization, tensor field visualization, flow visualization.*

1 Introduction

Many physical problems are currently visualized incompletely in terms of vector or scalar data because of a lack of proper tensor display techniques. Providing scientists with a methodology for visualizing 3-D second order tensor data can lead to new insights into these problems. Second order tensor fields are fundamental to many disciplines of engineering and physical sciences. Stresses and strains in solids, for example, are tensor fields. In fluid flows, stresses, viscous stresses, rate-of-strain, and momentum transfers are all described in terms of tensor data. Also, the steady-state Navier-Stokes equations describing gas flows involve only one quantity: a tensor field called *momentum flux density*. Table 1 gives the definition of some common 3-D tensor fields. It shows that tensor data are very rich in information content; they include diverse physical quantities such as pressure, kinetic energy density, mass density, velocity, and derivatives of the velocity field. Visualizing tensor fields provides a correlation between these quantities.

As a result of this wealth of highly multivariate information, tensor visualization is a challenging enterprise. Indeed, a 3-D second order tensor field $\mathbf{T}$ consists of a 3x3 array of scalar functions $\{T_{ik}\}$, $i,k = 1,2,3$ defined over a 3-D domain[1]. Independent visualization of those nine functions is possible but meaningless. This article presents a methodology based on the concept of a *hyperstreamline*, which is the simplest continuous *tensor* structure that can be extracted from a tensor field (as opposed to many other *scalar* or *vector* features).

In the next section, hyperstreamlines are introduced for the particular case of *symmetric* tensor fields $\mathbf{U} = \{U_{ik}\}$ whose individual components are related to each other by $U_{ik} = U_{ki}$ for $i,k = 1,2,3$. As seen in Table 1, symmetric tensor fields are very common in fluid flow studies. Then, a structural depiction of symmetric tensor fields is derived from the representation of a large number of hyperstreamlines. Finally, a methodology to visualize *unsymmetric* tensor data is provided by encoding an additional vector field along the trajectory of the hyperstreamlines.

[1] Useful information about tensor fields can be found in [Hal 91].

$v_{i,k} = \frac{\partial v_i}{\partial x_k}$	- velocity gradient (U)
$e_{ik} = v_{i,k} + v_{k,i}$	- rate-of-strain tensor (S)
$\sigma'_{ik} = \eta e_{ik}$	- viscous stress tensor (S)
$\sigma_{ik} = -p\delta_{ik} + \sigma'_{ik}$	- stress tensor (S)
$\Pi^r_{ik} = p\delta_{ik} + \rho v_i v_k$	- reversible momentum flux density tensor (S)
$\Pi_{ik} = \Pi^r_{ik} - \sigma'_{ik}$	- momentum flux density tensor (S)

[a] In non-Cartesian coordinate systems, covariant derivatives must be used instead.

[b] In compressible flows, there is an additional term involving the divergence of the velocity field.

Table 1: Tensor fields in fluid flows. p = pressure, ρ = mass density, v_i and v_k = velocity components, and η = viscosity. δ_{ik} is the Kronecker symbol. (U) = unsymmetric, (S) = symmetric.

2 Symmetric tensor fields and hyperstreamlines

Symmetric tensor fields $\mathbf{U} = \{U_{ik}\} = \{U_{ki}\}$ are very common in physics and engineering and their visualization is an important problem per se. Also, it is a necessary step for the display of general unsymmetric data, which will be addressed in the last section of this article.

A symmetric tensor $\mathbf{U}$ may be described by three orthogonal vector fields. Indeed, $\mathbf{U}$ has at every point $\overline{x}$ three real eigenvalues $\lambda^{(i)}$, $i = 1, 2$, or 3 ordered according to

$$\lambda^{(1)} \geq \lambda^{(2)} \geq \lambda^{(3)}$$

as well as three real and orthogonal unit eigenvectors $\overline{e}^{(i)}$ [1]. We consider the three orthogonal vectors $\overline{r}^{(i)}$ given by

$$\overline{r}^{(i)} = \lambda^{(i)}\overline{e}^{(i)} \qquad (1)$$

Because of the particular ordering of the eigenvalues, we refer to $\overline{r}^{(1)}$ as the *major eigenvector*, $\overline{r}^{(2)}$ as the *medium eigenvector*, and $\overline{r}^{(3)}$ as the *minor eigenvector*.

Visualizing $\mathbf{U}$ is fully equivalent to visualizing simultaneously the three vector fields $\overline{r}^{(i)}$, since they include all the *amplitude* information (the eigenvalues $\lambda^{(i)}$) and all the *directional* information (the unit eigenvectors $\overline{e}^{(i)}$) represented in matrix notation by the components U_{ik}. Furthermore, visualizing the three vectors $\overline{r}^{(i)}$ allows one to understand the behavior of the six independent components U_{ik} with little or no training [2].

Some of the early developed methods attempt to visualize these three vectors at each location by glyphs for using *point tensor icons*. Examples of such icons include ellipsoids having for principal axes the three vectors $\overline{e}^{(i)}$ or Haber's *tensor glyphs* [3, 4]. Point icons represent all the tensor information at a given location but their discrete nature does not reveal the underlying continuity of the data field. For this reason, Dickinson [5] used *tensor field lines* which are streamlines of one of the eigenvector fields $\overline{e}^{(i)}$. While emphasizing data continuity, tensor field lines are only *vector icons* and represent only partially the tensor field (this is analogous to representing a vector field by examining only one of its scalar components).

What is more desirable is a *line tensor icon* that represents all the tensor information along a 3-D path in space or, equivalently, that encodes a continuous distribution of ellipsoids along a given trajectory. For this purpose we generalize the vector notion of a streamline to the tensor concept of a *hyperstreamline*:

> a geometric primitive of finite size sweeps along one of the eigenvector fields $\overline{e}^{(i)}$ while stretching in the transverse plane under the combined action of the two other orthogonal eigenvector fields. The surface obtained by linking the stretched primitives at the different points along the trajectory is called a *hyperstreamline* and is color coded by means of a user-defined function of the three eigenvalues, generally the amplitude of the longitudinal eigenvalue.

The color and trajectory of a hyperstreamline fully represent the longitudinal eigenvector field and the cross-section encodes the two remaining transverse eigenvector fields. Thus, hyperstreamlines form a continuous representation of the whole tensor data along the trajectory. Hyperstreamlines are called *major*, *medium*, or *minor* depending on the longitudinal eigenvector field $\overline{e}^{(i)}$ that defines the trajectory.

Figures 1 and 2 illustrate the properties of hyperstreamlines for two elastic stress fields in a semi-infinite steel solid, and are described in detail below. The color scales for these and every other figure in this article are shown in Fig. 2.

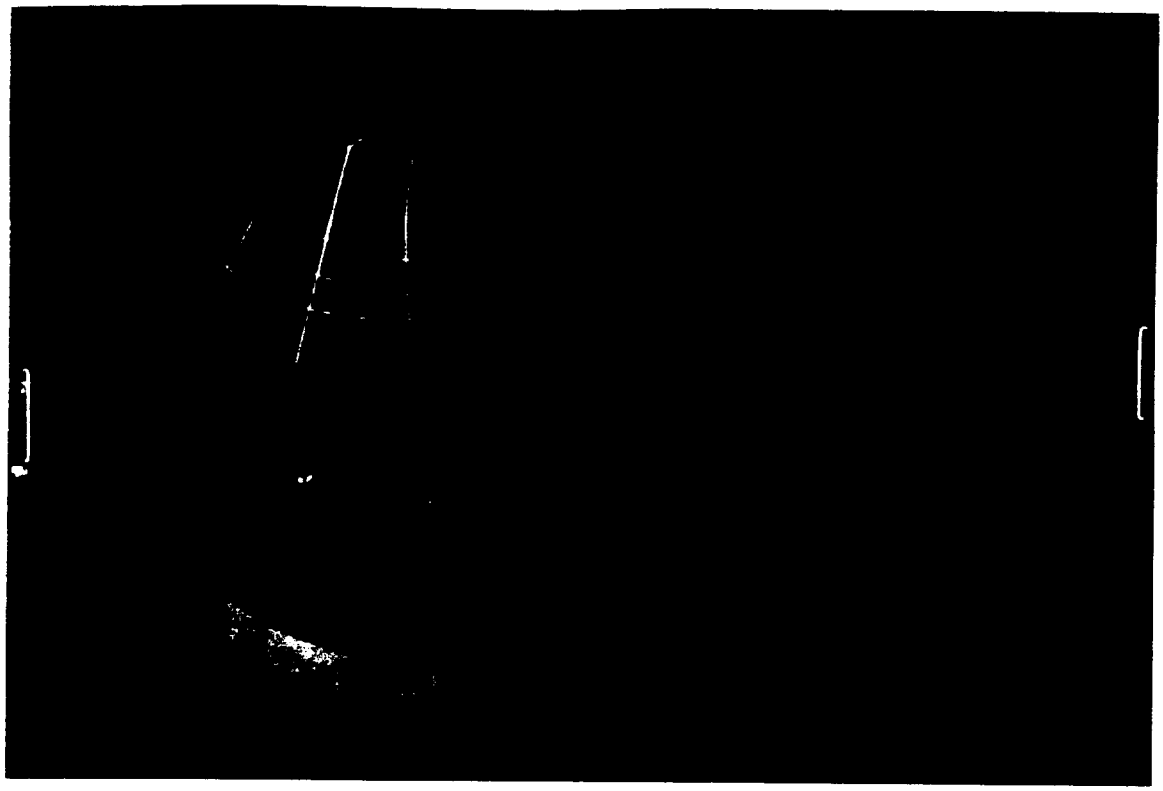

Figure 1: Stress tensor induced by two compressive forces. Hyperstreamline trajectories *(top)*; minor tubes, medium and major helices *(bottom)*; solenoidal property of a minor tube *(right)*. Color scale A of Fig. 2 is used.

2.1 Trajectory of a hyperstreamline

Hyperstreamline trajectories correspond to Dickinson's tensor field lines [5]; these patterns of lines show, for example, how forces propagate in a stress tensor field, and how the momentum is transferred in a momentum flux density tensor field. Figure 1(top) illustrates this phenomenon in an elastic stress tensor field induced by two compressive forces on the top surface of the cube. The lines propagating upward are along the most compressive direction (the minor eigenvector $\overline{v}^{(3)}$), and converge towards the regions of high stress where the forces are applied. Note the sudden divergence of close trajectories on each side of the plane of symmetry. Similarly, trajectories along the two other eigenvectors delineate a surface shown near the bottom face of the cube. This surface is everywhere perpendicular to the most compressive direction.

2.2 Cross-section of a hyperstreamline

Hyperstreamlines are further characterized by the geometry of their cross-section, i.e. the geometric primitive that sweeps along the trajectory. We consider two types of primitives: 1- a *circle* that stretches into an ellipse while sweeping and that generates a hyperstreamline called a *tube*; and 2- a *cross* that generates a hyperstreamline called a *helix*. Figure 1(bottom) shows two minor tubes propagating upward as well as four medium and major helices in the stress tensor field corresponding to Fig. 1(top). In a tube, the principal axes of each elliptical cross-section are along the transverse eigenvectors and have a length proportional to the magnitude of the transverse eigenvalues. The same property holds for a helix, whose arms are proportional to the transverse eigenvectors (helices owe their name to the spiraling pattern of their arms that can be observed in some cases). In this manner both directional and amplitude information are encoded along the trajectory. The local sign of the transverse eigenvalues can be detected by examining the singularities in the cross-section of the hyperstreamline. Indeed, the cross-section reduces to a single line or a point wherever one of the transverse eigenvalues changes sign.

Tubes and helices encode the same information about the tensor field, but some aspects of the data are better perceived with one hyperstreamline than with the other. Tubes, for instance, show better where the tensor is degenerate in the transverse plane, since recognizing that an ellipse is circular is easier than comparing the length of two perpendicular line segments. Further, if the tensor field is transversely degenerate in a whole region of space, helices are not adequate since in this case the direction of the transverse eigenvectors is not determined. Helices, on the other hand, provide better cues for perceiving precisely the directions of the transverse eigenvectors.

Four different stages of a minor tube in a stress tensor field are displayed in Fig. 2. The tensor field is similar to that of Fig. 1 but an additional tension force is added. In the top-left, the cross-section is circular, and the transverse stresses are equal in magnitude. The top-right shows an increasing anisotropy of the transverse stresses together with a decrease of the longitudinal eigenvalue (color). In the bottom-left, the cross-section is reduced to

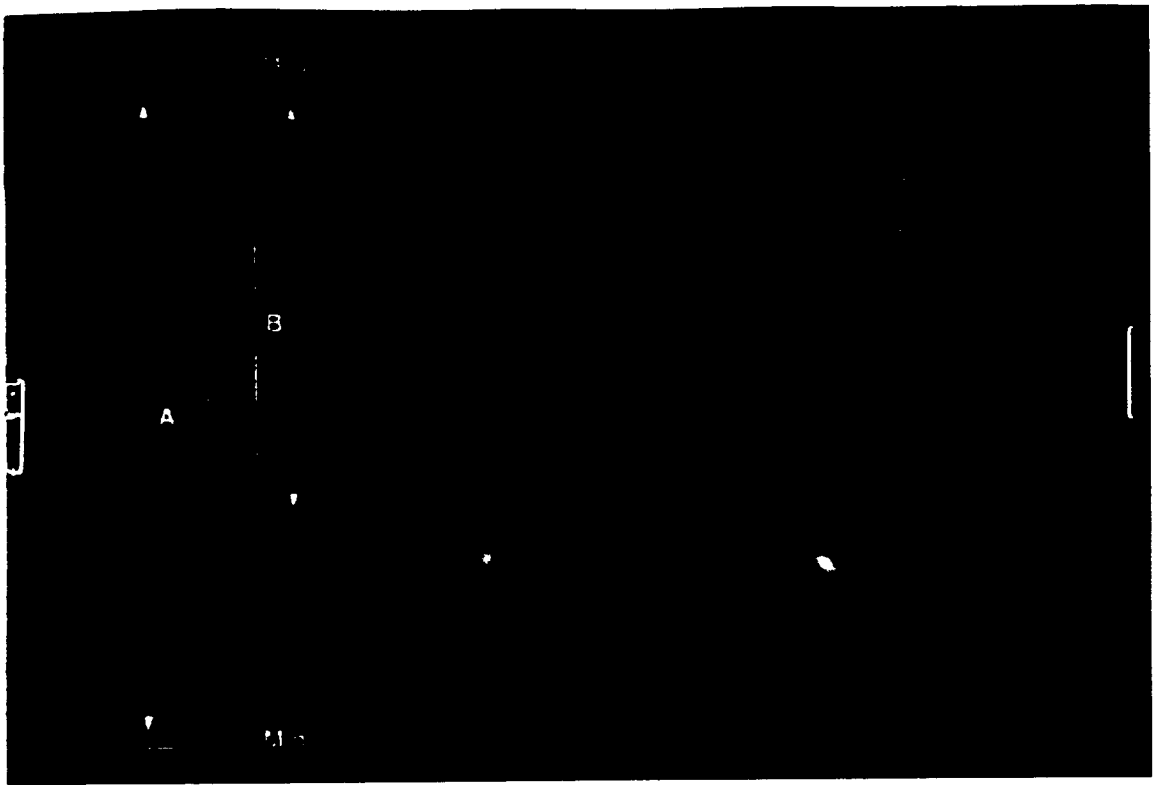

Figure 2: Four different stages of a minor tube in an elastic stress tensor field. Color scale A is used.

a straight line: one transverse eigenvalue is zero and the stresses are locally 2-D. In the bottom-right, the stresses are 3-D once again: the eigenvectors undergo a rapid rotation and a substantial stretching which reveals an important gradient of shear and pressure in the region.

Degenerate and singular points. Computing hyperstreamlines is complicated because degeneracies can occur along the trajectory at and in between the sampling points requested by the adaptive integration algorithm. We assume that the tensor field is smooth, i.e. that the direction of the longitudinal eigenvector is not likely to vary by more than a user-predefined angle between two successive sampling points, unless the trajectory just crossed a degeneracy involving the longitudinal eigenvalue. In this case, we search for the degeneracy between the last two sampling points and, if found, terminate the curve there. We can then jump the degeneracy and continue integrating in a selected eigendirection. The points where the transverse eigenvalues vanish are also detected and included to the curve in order not to miss a singularity of the cross-section of the hyperstreamline.

2.3 Solenoidal tensor fields

In our tensor fields, the hyperstreamlines have the additional property that the eigenvectors of color along the trajectory capture some behavior of neighboring hyperstreamlines. We define these tensor fields as *solenoidal* by analogy with the properties of solenoidal vector fields.

A vector field $\overline{v}$ is called *solenoidal* if it is divergence-free, i.e.

$$\sum_{i=1}^{3} \frac{\partial v_i}{\partial x_i} = 0$$

Examples of solenoidal vector fields include the vorticity or the velocity in steady-state incompressible flows. Much of the structure of solenoidal vector fields can be explained by their property of having a constant flux inside a streamtube [1]: the magnitude of the vector field must increase locally in regions where the streamlines converge towards each other and decrease where the streamlines diverge from each other.

By analogy, we define a tensor field $\mathbf{U}$ as *solenoidal* if it satisfies

$$\sum_{i=1}^{3} \frac{\partial U_{ik}}{\partial x_i} = 0 \qquad 2$$

for $k = 1, 2, 3$ which implies that the three vector fields obtained by multiplying $\mathbf{U}$ by any three constant orthogonal directions are solenoidal.

Solenoidal tensor fields are not rare mathematical objects. They are fundamental to fluid and solid-state mechanics. For example the stress tensor σ_{ik} in solids at rest (in regions where no external forces are applied) and the momentum flux density tensor Π_{ik} in gravity-free steady-state fluid flows both satisfy Eqn. 2 and are solenoidal tensor fields (the assumption of no gravity is common practice when computing gas flows). However, the stress and viscous stress tensors in fluid flows are not solenoidal.

Hyperstreamlines of solenoidal tensor fields have a convergence/divergence property analogous to the property of streamlines in solenoidal vector fields. More precisely, if $\lambda^{(1)}$ is the longitudinal eigenvalue of a hyperstreamline along the eigenvector $\overline{v}^{(1)}$ and if $\lambda^{(2)}$ and $\lambda^{(3)}$ are the two transverse eigenvalues, Eqn. 2 is equivalent to

$$\lambda^{(1)\prime} = K_{12}(\lambda^{(1)} - \lambda^{(2)}) + K_{13}(\lambda^{(1)} - \lambda^{(3)}) \qquad 3$$

Figure 3: Rake of major tubes of the momentum flux density tensor in the flow past an ogive cylinder. Color scale A of Fig. 2 is used.

where $\lambda^{(3)\prime}$ is the derivative of the longitudinal eigenvalue *along the trajectory* $\vec{y}$. K_{jj} and K_{kk} are geometric factors that are positive if neighboring hyperstreamlines along $\vec{e}^{(3)}$ converge in the corresponding transverse directions j or k and negative otherwise. Thus, when the longitudinal eigenvalue of a *major* hyperstreamline increases during its propagation ($\lambda^{(3)\prime} > 0$), neighboring *major* hyperstreamlines converge towards each other. Any divergence in one transverse eigendirection must be compensated by a stronger convergence in the other transverse eigendirection. The opposite property holds true for *minor* hyperstreamlines: an increasing longitudinal (minor) eigenvalue correlates with a global divergence of neighboring *minor* hyperstreamlines. If they converge in one transverse eigendirection, they must diverge more strongly in the other transverse eigendirection. Conversely, a decreasing longitudinal eigenvalue corresponds to diverging *major* hyperstreamlines and converging *minor* hyperstreamlines.

It follows, then, that encoding the longitudinal eigenvalue into the color of a hyperstreamline in a solenoidal tensor field gives information about the behavior of neighboring

hyperstreamlines. The figure at the beginning of this article illustrates this property for major tubes of the momentum flux density tensor in the flow past a hemisphere cylinder. The decrease of the longitudinal eigenvalue (color) is accompanied by diverging trajectories.

The former property explains why the minor hyperstreamlines in Fig. 1 converge towards the applied forces (quickly decreasing longitudinal eigenvalue) and why the major hyperstreamlines propagate mostly parallel to each other with an almost constant color. A close view of the sudden divergence of minor hyperstreamlines on one side of the plane of symmetry is given in Fig. 1(right). The local divergence of minor trajectories creates a sudden increase of the longitudinal eigenvalue counterintuitive to the notion that the minor eigenvalue should decrease uniformly when approaching one of the two applied compressive forces.

Figure 3 shows a rake of major tubes of the momentum flux density tensor in the flow past an ogive cylinder. The air flow comes in from a direction 5° to the left of the ogive axis and vortices are created in the wake of the body. Major tubes that become entangled in the vortices undergo a fast decrease in color while diverging from each other. In other regions of the flow, the color is constant and in some places it even increases slightly from orange to red. In these regions the apparent divergence of the tubes in the direction parallel to the surface of the body is compensated by a stronger convergence in the perpendicular direction. Both divergence and convergence exactly compensate each other in the tail between the two vortices.

2.4 The reversible momentum flux density tensor

A specific example of fluid flow analysis illustrates how hyperstreamlines may be used to correlate several different physical quantities. For the reversible part of the momentum flux density tensor, Π^r_{ik} (see Table 1), one may correlate pressure p, velocity direction $\overline{\mathrm{T}}_v$, and kinetic energy density k [2]. Indeed, the major eigenvalue of Π^r_{ik} is $\lambda^{(1)} = p + 2k$ and the corresponding unit eigenvector is the velocity direction $\overline{\mathrm{T}}_v$. The other eigenvalues are degenerate ($\lambda^{(2)} = \lambda^{(3)} = p$) in the whole space. It follows that only major tubes can be

Figure 4: Reversible momentum flux density tensor in the flow past a hemisphere cylinder. Color scale A of Fig. 2 is used.

used. Their trajectory is everywhere tangent to the velocity direction $\overline{\Gamma}_v$ and their cross-section is circular, with a diameter proportional to the pressure p. The color of the tubes is determined by the function

$$color \sim \frac{\lambda^{(1)} - 0.5(\lambda^{(2)} + \lambda^{(3)})}{2} = k \tag{4}$$

which represents the kinetic energy density k. Thus, the trajectory, diameter, and color of the major tubes encode the velocity direction, pressure and kinetic energy density, respectively.

Figure 4 shows Π^r_{ik} in the flow past a hemisphere cylinder. The direction of the incoming flow is 5° to the left of the hemisphere axis. The detachment at the end of the cylinder is clearly visible. The pattern of hyperstreamlines indicates that the momentum is transferred from the tip of the body to the end fairly uniformly with a globally decreasing kinetic energy as shown by color variations. However, there is a sudden change of kinetic energy (color) and pressure (diameter) associated with a significant variation of the direction of the first five tubes.

2.5 Color coding schemes

Usually, color encodes the longitudinal eigenvalue in order to represent the whole tensor data along the trajectory. In practice, the color coding scheme can be modified to reveal other aspects of the data. An example is the color coding function of Eqn. 4 which allows decoupling of pressure and kinetic energy density when visualizing the reversible momentum transfers in a flow. For stresses in solids or viscous stresses in fluids, color can be used to discriminate between compressive and tensile directions in the cross-section of a tube. This is done by coloring the tube according to

$$color \sim \cos(\varphi) \tag{5}$$

where φ is the angle between the normal $\overline{n}$ to the elliptical cross-section of a tube and the force $\overline{f} = \mathbf{U}\overline{n}$ acting on it. Figure 5 represents the same minor tube as in Fig. 2, but colored according to Eqn. 5. Red corresponds to $\varphi = 0°$ and indicates that the corresponding directions $\overline{n}$ are in pure tension. Blue indicates purely compressive directions ($\varphi = 180°$), and green reveals pure shear ($\varphi = 90°$).

When using the color function of Eqn. 5 for other tensor data, the meaning of compressive and tensile directions is lost. However, this scheme encodes the sign of the transverse eigenvalues: a principal direction of the elliptical cross-section is red if the corresponding eigenvalue is positive, and blue otherwise.

3 Structural depiction of symmetric tensor fields

Two factors limit the practicality of hyperstreamlines: 1) the resulting display depends on the initial conditions of integration and 2) a large number of hyperstreamlines produces visual clutter. The same problems arise in 3-D scalar and vector field visualization. For example, when visualizing a scalar field with isosurfaces, the final image depends on the particular isosurfaces chosen and only a few of them can be displayed simultaneously. Also, the conventional streamlines used in vector field visualization lead to a display dependent on the initial conditions of integration and the presence of too many streamlines clutters

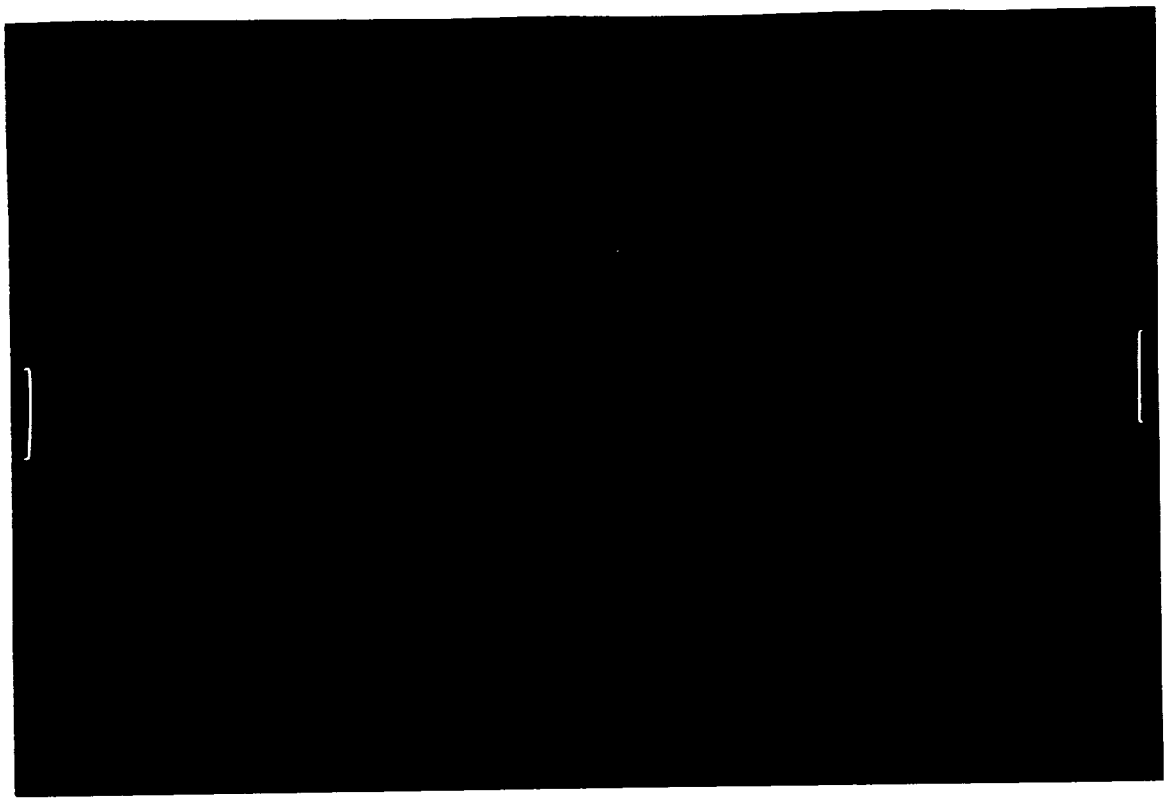

Figure 5: The minor tube of Fig. 2 colored as a function of the normal force. Color scale B of Fig. 2 is used.

the image. In the latter case, these problems are overcome by algorithms that extract automatically the vector field topology [7, 8]. These algorithms can be seen as a way of coding the collective behavior of a large set of vector streamlines. Analogous to these vector techniques, *a structural depiction of tensor data can be obtained by coding the collective behavior of a large number of hyperstreamlines.*

Consider the collection $\{HS^{(i)}\}$ of hyperstreamlines propagating along the eigenvector field $\overline{v}^{(i)}$ as given by Eqn. 1. Important features exist in both the trajectory and the cross-section of these hyperstreamlines. For example, the locus

$$\lambda^{(i)} = 0$$

is the set of the critical points[2] in the trajectory the hyperstreamlines $\{HS^{(i)}\}$. Further, the surface

$$\lambda^{(j)}\lambda^{(k)} = 0$$

[2] At a critical point of a vector field, the magnitude vanishes and the direction of the streamline is locally undefined. See Ref. [9] for a complete discussion of this topic.

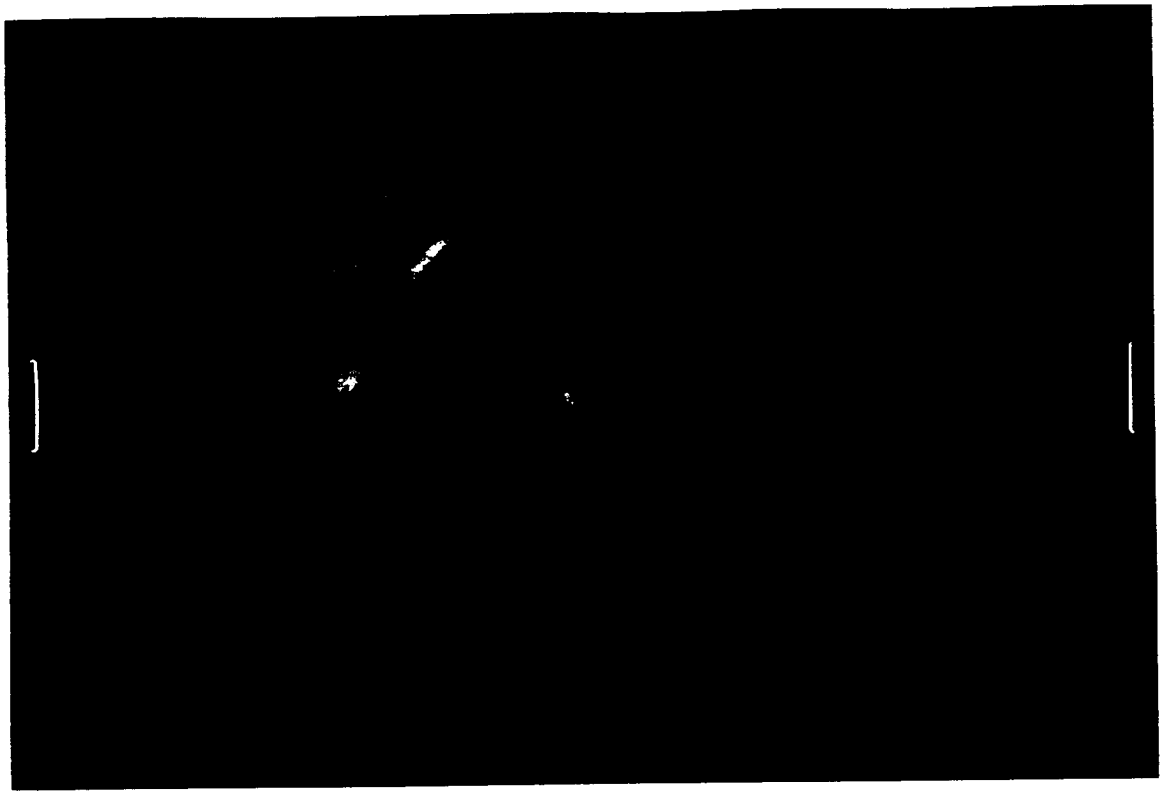

Figure 6: Structural depiction of the stress tensor of Fig. 1.

where $\lambda^{(j)}$ and $\lambda^{(k)}$ are the transverse eigenvalues, is the locus of points where the cross-section of the hyperstreamlines $\{HS^{(i)}\}$ is singular, i.e. is reduced to a straight line or a point. In general, a *surface of constant eccentricity* is the locus of points where the cross-section of each hyperstreamline in $\{HS^{(i)}\}$ has the same shape, regardless of its orientation and scaling. In particular, the locus

$$\lambda^{(j)} \pm \lambda^{(k)} = 0$$

is the set of points where the cross-section degenerates into a circle (zero eccentricity)[3].

A structural depiction of the stress tensor of Fig. 1 is given in Fig. 6. The yellow surface is the locus of critical points of the medium eigenvector $\overline{v}^{(2)}$ and the green surface represents the critical points of the major eigenvector $\overline{v}^{(1)}$. On both of these surfaces, the cross-section of each minor tube (four of them are shown) reduces to a straight line. On the blue surface, the transverse eigenvalues are opposite to each other and the cross-section is circular. Below the yellow surface, both transverse eigenvalues are positive and every transverse direction in the cross-section of the minor tubes is in tension. Above the yellow surface, the medium

[3]The locus $\lambda^{(j)} + \lambda^{(k)} = 0$ was omitted in Ref. [2].

eigenvalue becomes negative and some transverse directions are in tension while others are compressive. Inside the green surface, however, every transverse direction is in compression.

3.1 Stress and viscous stress tensors in fluid flows

Another example of structural depiction is given for the stress tensor σ_{ik} and the viscous stress tensor σ'_{ik} in fluid flows. As shown in Table 1, these two tensors differ only by an isotropic pressure component, implying that the unit eigenvectors of both tensor fields are identical. However, the eigenvalues of σ_{ik} are equal to the eigenvalues of σ'_{ik} minus a large pressure component. Table 1 also shows that visualizing σ'_{ik} is equivalent to visualizing the rate-of-strain tensor ϵ_{ik} in incompressible flows.

Hyperstreamlines of the stress tensor in the flow past a hemisphere cylinder are shown in Fig. 7(top) (the flow is the same as in Fig. 4). The major tubes in front are along the least compressive direction $\overline{v}^{(1)}$. Their trajectory shows how forces propagate from the region in front of the cylinder to the surface of the body. The cross-section of the tubes is circular, indicating that the pressure component of the stresses is dominant, as expected. However, the viscous stresses close to the body create a slightly anisotropic cross-section. On the yellow surface, the eccentricity is equal to 10%.

The helices are along the medium eigenvector field. They propagate mainly parallel to the cylinder surface and the orientations of their arms indicate a fairly constant direction of the two transverse eigenvectors. The third helix exhibits a more complex behavior, suggesting that the stress tensor is less uniform in the region of contact between the tubes and the body than in other parts of the flow.

Figure 7(bottom) shows the viscous stress tensor σ'_{ik} in the same flow. As expected, the trajectories are similar to those in Fig. 7(top), but removing the large isotropic pressure contribution dramatically enhances the anisotropy of the cross-section of the tubes. The surface corresponds to a constant eccentricity of 90% and is crossed twice by each tube.

Figure 7: Stress tensor *(top)* and viscous stress tensor *(bottom)* in the flow past a hemisphere cylinder. Color scale A of Fig. 2 is used.

4 Unsymmetric tensor fields

Hyperstreamlines are useful in visualizing *symmetric* tensor fields whose three eigenvector fields $\overline{v}^{(i)}$ given by Eqn. 1 are real and orthogonal. However, visualizing *unsymmetric* 3x3 tensor fields $\mathbf{T} = \{T_{ik}\}$ is more difficult because their eigenvectors $\overline{v}^{(i)}$ are generally complex and not orthogonal. A 3-D vector field visualization technique, the *stream polygon* [10], can reveal aspects of vector field gradients. It does not apply, however, to other kinds of unsymmetric data, and the tensor information, even for vector gradients, is only partially rendered.

In this section, we show that it is always possible to decompose unsymmetric tensor data into two components: a symmetric tensor field and a vector field. The symmetric tensor field is visualized with hyperstreamlines as before. However, in order to represent the complete (unsymmetric) tensor information, we need to encode the additional vector field along the trajectory. Depending of the physics involved, two reductions of the unsymmetric data are possible: a *symmetric / antisymmetric* decomposition or a *polar* decomposition.

4.1 Symmetric / antisymmetric decomposition

The tensor field can be decomposed into the sum of symmetric and antisymmetric components according to

$$\mathbf{T} = \frac{\mathbf{T} + \mathbf{T}^t}{2} + \frac{\mathbf{T} - \mathbf{T}^t}{2}$$

where $\mathbf{T}^t$ is the transpose of $\mathbf{T}$. The antisymmetric tensor has only three independent components that form a vector known as the *axial vector* [1, 11]. For instance, the velocity gradient in fluids is the sum of the rate-of-strain tensor ϵ_{ik} (symmetric) and the rate-of-rotation tensor (antisymmetric) which is half the vorticity vector.

Figure 9(top) shows a line tensor icon for unsymmetric data based on this decomposition. A hyperstreamline is integrated along one eigenvector field $\overline{r}^{(i)}$ of the symmetric tensor component and is color coded either according to the longitudinal eigenvalue or as in Eqn. 5. An additional ribbon is added *outside* of the tube surface in order to represent the axial vector. The ribbon position and width encode locally the vector component which is perpendicular to the trajectory. The color of the ribbon maps the angle between the axial vector and the direction of propagation of the tube according to color scale B of Fig. 2 (red is parallel, green is perpendicular, and blue is antiparallel). In Fig. 9(top) for example, color shows that the vector field is everywhere close to alignment with the direction of propagation. It is, however, not exactly aligned since the ribbon has a finite width.

When visualizing the velocity gradient in fluid flows, this icon shows the position of the vorticity with respect to the principal strains, which is an important factor for understanding turbulence [12].

4.2 Polar decomposition

An alternative reduction of the unsymmetric data is the polar decomposition [11], which is a generalization to tensors (or matrices in general) of the usual decomposition of a complex number into the product of an amplitude and a phase. Assume as in Fig. 8 that the tensor $\mathbf{T}$ at a given point $\overline{x}$ maps the vertices of a cube from an initial state to a final deformed state. This global deformation can be decomposed into more elementary transformations.

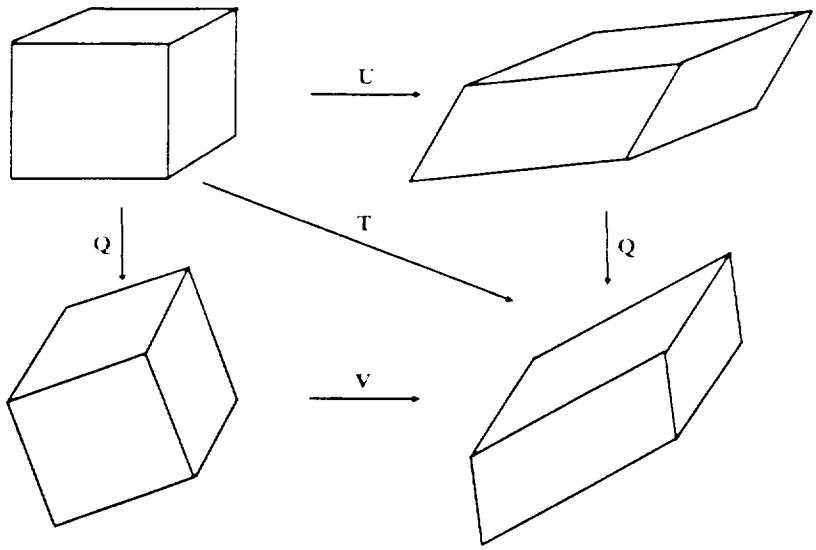

Figure 8: Polar Decomposition of unsymmetric data.

For example, one can first stretch the cube by a tensor **U** and then rotate the stretched rhomboid by an isometric transformation **Q** in order to reach the final state. Alternatively, one can first rotate the cube and then stretch it by the tensor **V**.

Mathematically, these are two equivalent ways of decomposing the unsymmetric data into the product of a stretch tensor **U** or **V** (the *amplitudes*) with an isometric transformation **Q** (the *phase*):

$$\mathbf{T} = \mathbf{QU} = \mathbf{VQ} \tag{6}$$

where both $\mathbf{U} = \sqrt{\mathbf{T}^t\mathbf{T}}$ and $\mathbf{V} = \sqrt{\mathbf{T}\mathbf{T}^t}$ are symmetric *positive definite* tensors, i.e. symmetric tensors having real and positive eigenvalues, and $\mathbf{Q} = \mathbf{T}\mathbf{U}^{-1}$ is an orthogonal tensor. It can be shown [11] that this decomposition is *unique* wherever $\det \mathbf{T} \neq 0$, i.e. there is a one-to-one correspondence between the matrix **T** and the set of matrices $\{\mathbf{Q}, \mathbf{U}, \mathbf{V}\}$. We will explain below how we handle points where $\det \mathbf{T} = 0$. From now on, we restrict our discussion to the first decomposition in Eqn. 6 without loss of generality.

Figure 9(bottom) shows a line tensor icon for **T** based on this decomposition. The symmetric tensor **U** is represented by a tube along one of its eigenvectors. In regions where $\det \mathbf{T} > 0$, the isometric tranformation **Q** is simply a rotation and is characterized by an

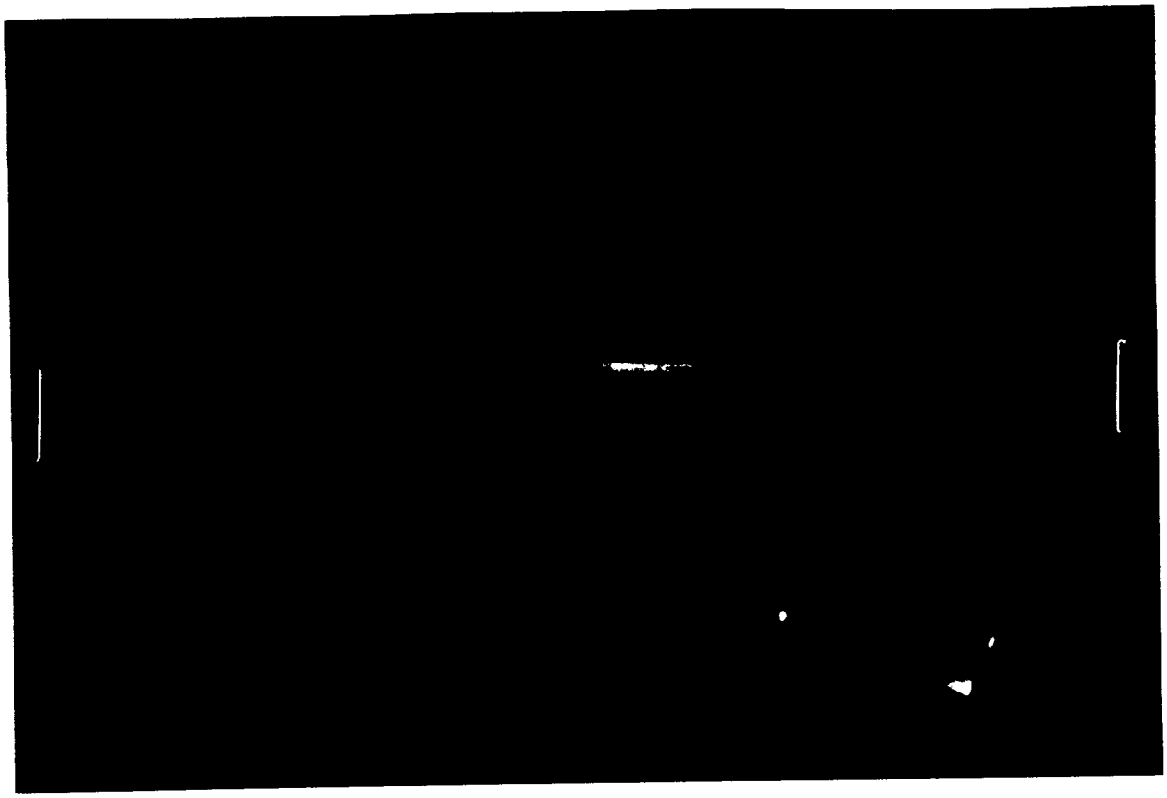

Figure 9: Examples of line tensor icons for two different unsymmetric tensor fields: symmetric / antisymmetric decomposition *(top)* and polar decomposition *(bottom)*. Color scales A and B of Fig. 2 are used for tubes and ribbons respectively.

angle θ ($0 \leq \theta \leq \pi$) and a unit axis of rotation $\overline{u}$. Thus, $\mathbf{Q}$ can be represented by the vector

$$\overline{r}^{(1)} = \theta \overline{u}$$

However, a rotation of angle θ about the axis $\overline{u}$ is physically identical to a rotation of angle $2\pi - \theta$ about the axis $-\overline{u}$. Thus, $\mathbf{Q}$ is also equivalent to the vector

$$\overline{r}^{(2)} = (2\pi - \theta)(-\overline{u})$$

To visualize $\mathbf{Q}$, two ribbons are added that represent the vectors $\overline{r}^{(1)}$ and $\overline{r}^{(2)}$, respectively. Note that in regions where $\det \mathbf{T} < 0$, the transformation $\mathbf{Q}$ involves an additional inversion in the direction of the rotation axis. A row of white pearls across the ribbons marks the onset of the inversion during the propagation, and a row of black pearls indicates its cancellation.

Singular points. In some points of the trajectory, the vectors $\overline{r}^{(1)}$ and $\overline{r}^{(2)}$ may not be defined. We then simply interpolate them between adjacent points in order to avoid

discontinuities in the ribbons. These singular points occur **a)** at the pearls where $\det \mathbf{U} = \det \mathbf{T} = 0$ ($\mathbf{U}$ is defined but not invertible and $\mathbf{Q}$ can not be computed) and **b)** where $\mathbf{Q}$ reduces to plus or minus the identity matrix (the rotation axis $\overline{n}$ is undefined and $\mathbf{T}$ is locally symmetric with all eigenvalues having the same sign). Thus, the assumption is that singularities are isolated points along the trajectories. This approach fails only if there is an entire subvolume where condition **a)** or **b)** occur. In the latter case, however, simple hyperstreamlines are useful since the data is symmetric.

5 Conclusions

The wealth of information contained in second order tensor data is extracted and rendered as hyperstreamlines. By representing continuously both the amplitude and the directional information typical of tensor data, hyperstreamlines reveal much of the physics involved in complicated processes that are otherwise only partially visualized in terms of vector or scalar functions. Hyperstreamlines are the simplest continuous tensor structures that can be extracted from symmetric or unsymmetric tensor fields, and coding their collective behavior is a first step in obtaining a structural depiction of tensor fields analogous to extracting vector field topology. Future work must be carried out to obtain more advanced structural depictions. To this aim, it might be necessary to focus on specific tensors each at a time and to use the known underlying physics and the resulting tensor properties within the framework of this article.

Acknowledgments

We wish to thank Yuval Levy for providing us with the fluid flow data sets and Paul Ning for his initial implementation of the Marching Cubes algorithm upon which our isosurface extraction algorithm is based. This work is supported by NASA under contract NCA 2-781 and by NSF under grant ECS8815815.

References

[1] A. I. Borisenko and I. E. Tarapov, *Vector and Tensor Analysis with Applications*, Dover Publications, New York, 1979.

[2] T. Delmarcelle and L. Hesselink, "Visualization of second order tensor fields and matrix data," in *Proceedings of IEEE Visualization '92*, pp. 316–323, IEEE Computer Society Press, Los Alamitos, CA., 1992.

[3] R. B. Haber, "Visualization techniques for engineering mechanics," *Computing Systems in Engineering*, vol. 1, no. 1, pp. 37–50, 1990.

[4] R. B. Haber and D. A. McNabb, "Visualization idioms: A conceptual model for scientific visualization systems," in *Visualization in Scientific Computing* (G. M. Nielson and B. Shriver, eds.), pp. 74–93, IEEE Computer Society Press, Los Alamitos, CA., 1990.

[5] R. Dickinson, "A unified approach to the design of visualization software for the analysis of field problems," in *SPIE Proceedings*, vol. 1083, pp. 173–180, SPIE, Bellingham, WA., 1989.

[6] T. Delmarcelle and L. Hesselink, "Visualizing tensor fields in fluid flows." In preparation.

[7] J. L. Helman and L. Hesselink, "Visualization of vector field topology in fluid flows," *Computer Graphics and Applications*, vol. 11, no. 3, pp. 36–46, 1991.

[8] A. Globus, C. Levit, and T. Lasinski, "A tool for visualizing the topology of three-dimensional vector fields," in *Proceedings of IEEE Visualization '91*, pp. 33–40, IEEE Computer Society Press, Los Alamitos, CA., 1991.

[9] M. S. Chong, A. E. Perry, and B. J. Cantwell, "A general classification of three-dimensional flow fields," *Phys. Fluids A*, vol. 2, no. 5, pp. 765–777, 1990.

[10] W. J. Schroeder, C. R. Volpe, and W. E. Lorensen, "The stream polygon: a technique for 3-d vector field visualization," in *Proceedings of IEEE Visualization '91*, pp. 126–132, IEEE Computer Society Press, Los Alamitos, CA., 1991.

[11] D. C. Leigh, *Nonlinear Continuum Mechanics*. McGraw-Hill Book Company, New York, 1968.

[12] W. T. Ashurst, A. R. Kerstein, R. M. Kerr, and C. H. Gibson, "Alignment of vorticity and scalar gradient with strain rate in simulated navier-stokes turbulence," *Phys. Fluids*, vol. 30, pp. 2343–2353, Aug. 1987.

Biographies

Thierry Delmarcelle is a research assistant in the Fourier Optics and Optical Diagnostics Laboratory at Stanford, where he is completing work on a PhD in applied physics. His dissertation is on the representation and interpretation of tensor fields, and his other research interests include flow visualization, computer graphics, and color perception.

Delmarcelle received a degree in physics engineering from the Faculté des Sciences appliquées of the Université Libre de Bruxelles (Brussels, Belgium) in 1988 and a MS in applied physics from Stanford in 1991.

Delmarcelle can be reached at the Department of Applied Physics, Stanford University, Stanford, CA, 94305-4090.

Lambertus Hesselink holds a joint appointment as Professor in the electrical engineering and aeronautics and astronautics departments at Stanford University. He has served on several scientific advisory committees for industry and the U.S. Government, most recently on the advisory committee for the Hubble Space Telescope. His research interests include nonlinear optics, optical phase conjugation, optical signal processing, optical computing, optical diagnostics, and 3D image processing.

Hesselink received a BS in applied mechanics and a separate BS in applied physics from the Twente Institute of Technology in the Netherlands. He received his MS and PhD from the California Institute of Technology. He is a fellow of the Optical Society of America, and has published over 110 journal articles.

Hesselink can be reached at the Department of Aeronautics and Astronautics, Durand Building, Room 353, Stanford University, Stanford, CA, 94305-4035.